Journal of Computational Physics **178,** 196–209 (2002)
doi:10.1006/jcph.2002.7029, available online at http://www.idealibrary.com on IDEAL®

Simulation of Coupled Diffusion of Impurity Atoms and Point Defects under Nonequilibrium Conditions in Local Domain

O. I. Velichko,* V. A. Dobrushkin,† A. N. Muchynski,‡ V. A. Tsurko,§ and V. A. Zhuk‡

*Belarusian State University of Informatics and Radioelectronics, 6 P. Brovka Street, Minsk 220027, Belarus; †Brown University, Division of Applied Mathematics, Providence, Rhode Island 02912; ‡Silvaco Data Systems Inc., 4701 Patrick Henry Doctor Building 2, Santa Clara, California 95054; and §National Academy of Sciences, Institute of Mathematics, 11 Surganova Street, Minsk 220072, Belarus

E-mail: †dobrush@cfm.brown.edu

Received October 14, 1999; revised May 15, 2001

A two-dimensional model of doping of the active regions in semiconductor devices by means of ion implantation and thermal annealing is stated and analyzed. Radiation enhanced diffusion of impurity atoms during high temperature implantation of hydrogen ions is also considered. An economic finite difference method for solving the obtained system of diffusion equations is developed and numerical computations of the diffusion processes are carried out. © 2002 Elsevier Science (USA)

Key Words: coupled diffusion; point defect; rapid thermal annealing; radiation enhanced diffusion.

1. INTRODUCTION

In advanced IC fabrication, ion implantation is widely used for local doping of semiconductor substrates. The conventional implantation of dopant atoms into silicon at room temperatures produces a large amount of nonequilibrium radiation defects which are nonuniformly distributed in the implanted layer. Therefore, thermal processing is needed for radiation defect annealing and activation of the dopants [1]. The diffusion redistribution of all previously formed layers occurs during annealing and in many cases the extreme electrical parameter values of a device are hard to obtain. Hence, it is essential to investigate specific processing of a semiconductor substrate, which provides the local transformation of the previously selected doping layer in the strictly assigned direction. Local radiation enhanced diffusion of impurity atoms is one of the required processes. Such a local diffusion occurs during the implantation of hydrogen ions at substrate temperatures above 500°C. It is high temperature implantation of hydrogen ions that attracts our attention. First

0021-9991/02 $35.00

of all, in contrast to heavy particle bombardment, hydrogen implantation does not cause the formation of the stable radiation defects. For light ions and in low doses, ion damage can be compared to electron irradiation damage [2]. This means that generated defects are annealed either during implantation or during subsequent low temperature annealing [3]. Secondly, undesirable defects at the interface and in the bulk of the semiconductor can be passivated by the injection of hydrogen atoms into the silicon substrate [4, 5]. Thirdly, low values of hydrogen ion straggling provide a generation of point defects and, consequently, radiation enhanced diffusion in a very small region. A change of hydrogen implantation energy in the range 10 . . . 200 keV causes a local transformation of impurity distribution profiles in depth up to 2 μm.

In this paper, a two-dimensional model of active areas formation in semiconductor devices is formulated. It is assumed that the most current fabrication processes are used, including ion implantation, rapid thermal annealing, and radiation enhanced diffusion of dopant atoms during high temperature hydrogen implantation. The proposed model differs from previous published models of dopant diffusion in silicon [6–8]. The thermal diffusion of donor and acceptor impurities was considered in [7] while models of transient enhanced diffusion during annealing of ion-implanted layers were discussed in [6, 8]. In the present paper, we take into account both the radiation enhanced diffusion during a hydrogen ion bombardment at elevated substrate temperatures and the transient enhanced diffusion during the annealing of ion-implanted layers. The proposed model differs essentially from other models of radiation enhanced diffusion [9, 10] because the different charge states of the diffusing species and the influence of the internal electric field are taken into account. In addition, the proposed model describes a simultaneous radiation enhanced diffusion of several dopants in silicon.

Based on finite-difference approximations, an economic numerical method was developed to solve the initial boundary value problem for the diffusion equation. Such an approach allows us to reduce the vector partial differential equation to a nonlinear system of algebraic equations. Using the formulated generalized model, one develops and uses numerical methods for the two-dimensional simulation of transient enhanced diffusion during the annealing of ion implanted layers and for the simulation of radiation enhanced diffusion during high temperature implantation of hydrogen ions. This enables the prediction and calculation for various doping processes in the fabrication of advanced silicon devices.

2. FORMULATION OF PROBLEM

We assume that impurity transport, including the case of radiation enhanced diffusion during high temperature implantation of hydrogen ions, is carried out by means of formation, migration, and dissociation of "impurity atom—intrinsic point defect" pairs. As follows from [11, 12], the diffusion equation can be written in the matrix form

$$\partial C^T/\partial t = \sum_{i=1}^{2} \frac{\partial}{\partial x_i}\left[D(\chi)\frac{\partial N^C}{\partial x_i} + D^N(\chi, N^C)\frac{\partial \chi}{\partial x_i}\right], \tag{1}$$

where C^T, N^C, and χ are the vectors; D and D^N are the diagonal $n \times n$ matrices. The components of the vector of total concentration $C^T = (C_1^T, C_2^T, \ldots, C_n^T)$ are represented as $C_\alpha^T = C_\alpha + C_\alpha^{AC}$, where C_α is the concentration of electrically active impurity of species α and C_α^{AC} is the concentration of impurity atoms of species α, incorporated into clusters.

Here and below, $\alpha = 1, \ldots, n$. The components of the vector N^C are defined by the following expressions: $N_\alpha^C = \tilde{C}_\alpha C_\alpha$, $\tilde{C}_\alpha = C^X / C_i^X$, where C^X and C_i^X are the concentration of intrinsic point defects in the neutral charge state and the thermal equilibrium value of this concentration, respectively. We assume that

$$\tilde{C}_\alpha = \begin{cases} C^{VX}/C_i^{VX}, & \text{if vacancies } V \text{ are responsible for the diffusion} \\ & \quad \text{of the dopant atoms of species } \alpha, \\ C^{IX}/C_i^{IX}, & \text{in the case of the diffusion by means of self-interstitials.} \end{cases}$$

The components of the vector χ have the form $\chi_\alpha = (N_T + \sqrt{N_T^2 + 4n_i^2})/(2n_i)$. Here N_T is the difference between the concentration of the donors and the concentration of the acceptors if we consider a diffusion of the donors. Otherwise, N_T is the difference between the concentration of the acceptors and the concentration of the donors if we describe a diffusion of acceptor impurities. The parameter n_i is the intrinsic carrier concentration. The diagonal elements of the matrices D and D^N are

$$D_\alpha(\chi_\alpha) = D_{i,\alpha} \frac{1 + \beta_{1,\alpha}\chi_\alpha + \beta_{2,\alpha}\chi_\alpha^2}{1 + \beta_{1,\alpha} + \beta_{2,\alpha}}, \quad D_\alpha^N\left(\chi_\alpha, N_\alpha^C\right) = \frac{D_\alpha N_\alpha^C}{\chi_\alpha}.$$

Here D_α and $D_{i,\alpha}$ are the effective diffusivities and the intrinsic diffusivities of impurity atoms, respectively; $\beta_{1,\alpha}$ and $\beta_{2,\alpha}$ are empirical constants which describe the relative contribution of single and double charged defects to the diffusion process. The boundary conditions are

$$D(\chi)\frac{\partial N^C}{\partial \mathbf{n}} + D^N(\chi, N^C)\frac{\partial \chi}{\partial \mathbf{n}} = 0, \tag{2}$$

where $\mathbf{n}$ is the unit outward normal to the boundary of the domain. The initial conditions are

$$C^T(\mathbf{x}, 0) = C_0(\mathbf{x}), \quad \mathbf{x} = (x_1, x_2), \tag{3}$$

where $C_0(\mathbf{x})$ is the initial impurity distribution function. In the case of ion implantation, C_0 depends on published parameters [13].

The system of diffusion equations (1) has to be solved simultaneously with corresponding defect diffusion equations. In general, the defect diffusion is described by the Eq. [14]

$$\sum_{i=1}^{2} \frac{\partial}{\partial x_i}\left[D_\alpha^*(\chi_\alpha)\frac{\partial \tilde{C}_\alpha}{\partial x_i}\right] - \frac{\tilde{C}_\alpha}{\tau_\alpha^*(\chi_\alpha)} + \frac{g_{\alpha i} + g_\alpha(\mathbf{x})}{C_{\alpha^i}^X} = 0, \tag{4}$$

where $D_\alpha^*(\chi_\alpha) = D_{\alpha i}^* \tilde{D}_\alpha(\chi_\alpha)$, $\tau_\alpha^*(\chi_\alpha) = \tau_{\alpha i}\tilde{\tau}_\alpha(\chi_\alpha)$. Here τ_α^* has a meaning of effective defect lifetime and g_α is the summarized rate of generation of vacancies or self-interstitials in different charge states. We assume that the generation of nonequilibrium vacancies or self-interstitials can occur as a result of ion bombardment, crystal deformation, or radiation damage annealing. The magnitudes $D_{\alpha i}^*$, $\tau_{\alpha i}$, and $g_{\alpha i}$ are the values of functions D_α^*, τ_α^*, and g_α in an intrinsic semiconductor. We omit the index α further for simplicity.

Dividing the equation of defect diffusion by D_i^* and introducing the average diffusion length of defects $l_i = \sqrt{D_i^* \tau_i}$, we obtain

$$\sum_{i=1}^{2} \frac{\partial}{\partial x_i}\left[\tilde{D}\frac{\partial \tilde{C}}{\partial x_i}\right] - \frac{\tilde{C}}{l_i^2 \tilde{\tau}} + \frac{\tilde{C}_g}{g_i C_i^X D_i^*} = 0, \quad \tilde{C}_g = 1 + g(\mathbf{x})/g_i.$$

This equation yields the form

$$-1/l_i^2 + 1/\left(g_i C_i^X D_i^*\right) = 0$$

in the bulk of the semiconductor since it is only here that the thermal generation of point defects occurs ($g(x) = 0$). Therefore, the concentration of defects and the effective defect lifetime are equal to the equilibrium defect concentration and to the equilibrium defect lifetime, respectively ($C^X = C_i^X$ and $\tau^* = \tau_i$). Substitution of the expression $l_i^2 = g_i C_i^X D_i^*$ leads to the following defect diffusion equation:

$$\sum_{i=1}^{2} \frac{\partial}{\partial x_i}\left[\tilde{D}\frac{\partial \tilde{C}}{\partial x_i}\right] - \frac{\tilde{C}}{l_i^2 \tilde{\tau}} + \frac{\tilde{C}_g}{l_i^2} = 0.$$

Note that the concentration of impurity is comparable with n_i, the intrinsic carrier concentration, in the case of radiation enhanced diffusion. The effective diffusivity of defects $\tilde{D} = 1$ and the defect diffusion equation (4) becomes

$$\Delta \tilde{C} - \frac{\tilde{C}}{l_i^2} + \frac{\tilde{C}_g}{l_i^2} = 0. \tag{5}$$

Equation (5) is subject to the general boundary conditions

$$w_1 \partial \tilde{C}/\partial \mathbf{n} + w_2 \tilde{C} = w_3, \tag{6}$$

where w_1, w_2, w_3 are some coefficients related to the boundary conditions.

In the case of ion implantation, the generation rate of nonequilibrium point defects, $g(\mathbf{x})$, can be approximately represented by the analytical expression [3]:

$$g(\mathbf{x}) = \frac{G(x_1)}{2}\left[\operatorname{erf}\left(\frac{x_2 + a}{\sqrt{2}\Delta y^d}\right) - \operatorname{erf}\left(\frac{x_2 - a}{\sqrt{2}\Delta y^d}\right)\right], \quad \operatorname{erf}(x) = \frac{2}{\sqrt{\pi}}\int_0^x e^{-t^2}\,dt,$$

$$G(x_1) = \frac{p^d}{\sqrt{2\pi}\,\Delta R_p^d} \exp\left[-\frac{\left(x_1 - R_p^d\right)^2}{2\left(\Delta R_p^d\right)^2}\right].$$

Here p^d is the dose of point defects generated by means of hydrogen ion implantation per second, R_p^d is the average depth of the defect generation rate distribution, ΔR_p^d is the straggling of the defect generation rate distribution, and Δy^d is the lateral standard deviation for defect generation [13]. To further simulate the evolution of the defect subsystem, we will also use the parameter $\tilde{g} = p^d/(\sqrt{2\pi}\,\Delta R_p^d g_i)$, which represents a combination of these quantities.

The simulation domain is the flat section of a substrate perpendicular to its surface, $\tilde{G} = \{0 \le x_1 \le l_1,\ 0 \le x_2 \le l_2\}$ is the rectangle with the sides l_1 and l_2. $\Gamma = \bigcup_{\nu=1}^{4} \Gamma_\nu$ is its boundary, $G = \tilde{G} \backslash \Gamma$ (Fig. 1).

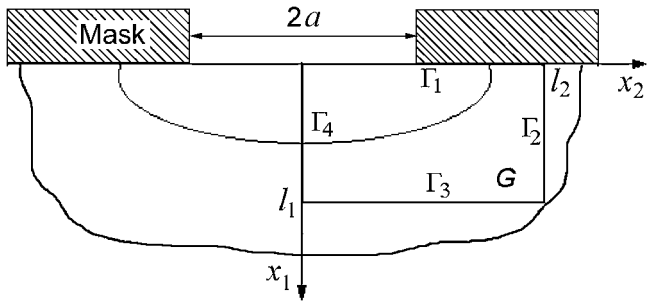

FIG. 1. Cross section of doped semiconductor structure.

3. NUMERICAL METHOD

Equations (1)–(3) are reduced to a more convenient form in order to facilitate the derivation of the numerical procedure, namely,

$$\partial\varphi(u)/\partial t = \sum_{i=1}^{2} \frac{\partial}{\partial x_1}\left[k_1(u)\frac{\partial u}{\partial x_i} + k_2(u)\frac{\partial r(u)}{\partial x_i}\right], \quad \mathbf{x} \in G, \quad t > 0, \tag{7}$$

$$k_1(u)\partial u/\partial \mathbf{n} + k_2(u)\partial r(u)/\partial \mathbf{n} = 0, \quad \mathbf{x} \in \Gamma, \quad t > 0, \tag{8}$$

$$u(\mathbf{x}, 0) = u_0(\mathbf{x}), \quad \mathbf{x} \in \tilde{G}. \tag{9}$$

Here $u, \varphi(u), r(u)$, and u_0 are the n-dimensional vectors, $k_1(u)$ and $k_2(u)$ are the diagonal $n \times n$ matrices whose components are $u_\alpha = N_\alpha^C, \varphi_\alpha(u_\alpha) = C_\alpha^T(C_\alpha) = C_\alpha^T(u_\alpha/\tilde{C}), r_\alpha(u) = \chi_\alpha(u/\tilde{C}), \quad u_{0,\alpha}(\mathbf{x}) = (C_\alpha^T)^{-1}(C_{0,\alpha}(\mathbf{x}))\tilde{C}, \quad k_{1,\alpha}(u) = D_\alpha(\chi_\alpha) = D_\alpha(r_\alpha(u)), \quad k_{2,\alpha}(u) = D_\alpha^N(\chi_\alpha, u_\alpha) = D_\alpha^N(r_\alpha(u), u_\alpha)$.

In order to solve the boundary value problem, an irregular rectangular grid is introduced in $\bar{G}$. The solution is determined at the mesh points of this grid. We use mobile meshes adapted for impurity distributions to provide fast calculations. A known mesh technique [15] was applied to generate the mesh points to solve numerically the boundary value problem.

We set a time mesh $\omega_\tau = \{t_0 = 0,\ t_j = \sum_{k=1}^{j} \tau_k,\ j = 1, 2, \ldots, j_0,\ \tau_k > 0\}$, where τ_j is the monotonically increasing step. A spatial mesh has the form: $\bar{\omega}_h = \{0 \le x_{1,i_1} \le l_1, 0 \le x_{2,i_2} \le l_2, h_{\beta,i_\beta} = x_{\beta,i_\beta} - x_{\beta,i_\beta-1}, i_\beta = 1, 2, \ldots, N_\beta, \beta = 1, 2\}, \omega_h = \bar{\omega}_h \backslash \gamma_h$ is the set of the inner mesh points, γ_h is the set of boundary mesh points, $\gamma_{h,\beta}$ is the set of boundary mesh points in the x_β-direction.

The economic algorithms are important for two-dimensional simulation. The splitting method [16] is one of the methods, which is suitable in our case since it provides fast computations.

We define the intermediate time layer $t_{j-0.5} = \tau_{j-1} + \tau_j/2$. Then we assign to Eq. (7) the sequence of one-dimensional differential equations

$$\frac{1}{2}\frac{\partial\varphi(v_{(1)})}{\partial t} = \frac{\partial}{\partial x_1}\left[k_1(v_{(1)})\frac{\partial v_{(1)}}{\partial x_1} + k_2(v_{(1)})\frac{\partial r(v_{(1)})}{\partial x_1}\right], \quad t_{j-1} < t \le t_{j-0.5}, \tag{10}$$

$$\frac{1}{2}\frac{\partial\varphi(v_{(2)})}{\partial t} = \frac{\partial}{\partial x_2}\left[k_1(v_{(2)})\frac{\partial v_{(2)}}{\partial x_2} + k_2(v_{(2)})\frac{\partial r(v_{(2)})}{\partial x_2}\right], \quad t_{j-0.5} < t \le t_j. \tag{11}$$

We use the values of the vector u from the previous time step as the initial conditions for (10). Similarly, we specify the initial conditions for Eq. (11) as the values of the vector $v_{(1)}$ at $t_{j-0.5}$, i.e., $v_{(1)}(\mathbf{x}, t_{j-1}) = u(\mathbf{x}, t_{j-1})$, $v_{(2)}(\mathbf{x}, t_{j-0.5}) = v_{(1)}(\mathbf{x}, t_{j-0.5})$. Then the boundary conditions for Eqs. (10) and (11) in the rectangular domain $\bar{G}$ are

$$k_1\big(v_{(1)}\big)\frac{\partial v_{(1)}}{\partial x_1} + k_2\big(v_{(1)}\big)\frac{\partial r\big(v_{(1)}\big)}{\partial x_1} = 0, \quad \mathbf{x} \in \Gamma_\nu, \quad \nu = 1, 3, \tag{12}$$

$$k_1\big(v_{(2)}\big)\frac{\partial v_{(2)}}{\partial x_2} + k_2\big(v_{(2)}\big)\frac{\partial r\big(v_{(2)}\big)}{\partial x_2} = 0, \quad \mathbf{x} \in \Gamma_\nu, \quad \nu = 2, 4. \tag{13}$$

The values of $v_{(2)}$ are used to estimate the solution of problems (7)–(9). The quantities y, $y_{(1)}$, and $y_{(2)}$ will be called approximate values of the vectors u, $v_{(1)}$, and $v_{(2)}$, respectively. We define the difference derivative in the direction x_β as

$$y_{(\beta),\bar{x}_\beta,i_\beta} = \big(y_{(\beta),i_\beta} - y_{(\beta),i_\beta-1}\big)/h_{\beta,i_\beta}, \quad y_{(\beta),\hat{x}_\beta,i_\beta} = \big(y_{(\beta),i_\beta+1} - y_{(\beta),i_\beta}\big)/\hbar_{\beta,i_\beta},$$
$$\varphi\big(y_{(\beta)}\big)_{\bar{t}} = \big(\varphi\big(y_{(\beta)}\big)^{j+\beta/2} - \varphi\big(y_{(\beta)}\big)^{j+(\beta-1)/2}\big)/\tau_j,$$

$\hbar_{\beta,i_\beta} = 0.5(h_{\beta,i_\beta+1} + h_{\beta,i_\beta})$. Here, the second fixed index in the above difference expressions is omitted.

We replace the system of differential equations (10), (12) on the mesh $\bar{\omega}_h$ for $i_2 = 0, 1, \ldots, N_2$ by the difference equations:

$$\varphi\big(y_{(1)}\big)_{\bar{t},i_1} = \big(a_{11}\big(y_{(1)}\big)y_{(1),\bar{x}_1}\big)_{\hat{x},i_1} + \big(a_{21}\big(y_{(1)}\big)b\big(y_{(1)}\big)_{\bar{x}_1}\big)_{\hat{x}_1,i_1},$$
$$i_1 = 1, 2, \ldots, N_1 - 1,$$
$$0.5h_{1,1}\varphi\big(y_{(1)}\big)_{\bar{t},0} = a_{11}\big(y_{(1)}\big)y_{(1),\bar{x}_1,1} + a_{21}\big(y_{(1)}\big)b\big(y_{(1)}\big)_{\bar{x}_1,1},$$
$$-0.5h_{1,N_1}\varphi\big(y_{(1)}\big)_{\bar{t},N_1} = a_{11}\big(y_{(1)}\big)y_{(1),\bar{x}_1,N_1} + a_{21}\big(y_{(1)}\big)b\big(y_{(1)}\big)_{\bar{x}_1,N_1}.$$

Here the matrices $a_{11}(y)$, $a_{21}(y)$, and the vector $b(y)$ are determined by the formulas:

$$a_{11}\big(y_{(1),i_1,i_2}\big) = 0.5\big(k_1\big(y_{(1),i_1-1,i_2}\big) + k_1\big(y_{(1),i_1,i_2}\big)\big),$$
$$a_{21}\big(y_{(1),i_1,i_2}\big) = 0.5\big(k_2\big(y_{(1),i_1-1,i_2}\big) + k_2\big(y_{(1),i_1,i_2}\big)\big),$$
$$b\big(y_{(1),i_1,i_2}\big) = r\big(y_{(1),i_1,i_2}\big).$$

In a similar manner we replace the system of differential equations (11), (13) by the difference equations for $y_{(2)}$. The values of $y_{(2)}^j$, $j = 1, 2, \ldots, j_0$ are used as approximate values to the solution of the problem (7)–(9). Note that the approximate solution of the initial boundary value problem (1)–(3) is $\varphi(y_{(2)})$.

The solution of the system of nonlinear difference equations is obtained using an iterative process. The calculation of the next iterative approximation is reduced to the solution of a sytem of linear algebraic equations with a tridiagonal matrix using the sweep method.

For the application of the proposed numerical method it is necessary to know distributions of defects. The equation of the defect diffusion (5) has an analytical solution in a one-dimensional case [14, 17]. In the two-dimensional case we use a finite difference method [18] to determine the solution of the elliptic equation (5). Replacing the differential operators

on the mesh ω_h by the appropriate difference analogues, we obtain

$$z_{x_1\hat{x}_1} + z_{x_2\hat{x}_2} - qz = -f_{i_1,i_2}, \quad x \in \omega_h. \tag{14}$$

Here z is the approximate solution of Eq. (5), $q = 1/l_i^2$, $f_{i_1,i_2} = \tilde{C}_g(x_{1,i_1}, x_{2,i_2})/l_i^2$. The system of equations (14) is subject to the relevant boundary conditions and the approximation at the corners of the grid is of special kind [19]. We use the direct method of matrix sweep for solving systems of linear algebraic equations.

The correctness and short running time of the proposed algorithm was established by the verification of the values of the solutions at various parameters of calculation (steps of the grid in space and time), comparison of two-dimensional calculations with the one-dimensional calculation in the direction x_1, comparison with other methods, for example, uneconomic methods, and check of the total amount of impurities before and after annealing.

4. PROCESS SIMULATION

A simulation of the defect-impurity system requires the estimation of the diffusion equation coefficients. For parameter estimations, the one-dimensional modeling of ion-implanted arsenic redistribution during rapid thermal annealing and simulation of radiation enhanced diffusion of phosphorus during high temperature implantation of hydrogen ions were carried out. Using the actual values of the model parameters, we have performed a two-dimensional model of doping processes for fabrication of metal-insulator-semiconductor field-effect transistors (MISFET) based on impurity ion implantation, thermal annealing, and high temperature implantation of hydrogen ions. The nonuniformity of point defect distributions was taken into consideration in the simulation process. We assumed that nonuniform distributions were formed due to the absorption of defects on the surface and point defect generation by ion implantation. In Fig. 2 the results of simulation for ion-implanted arsenic redistribution after rapid thermal annealing are shown. The appropriate experimental data were taken from [20]. The arsenic implantation energy

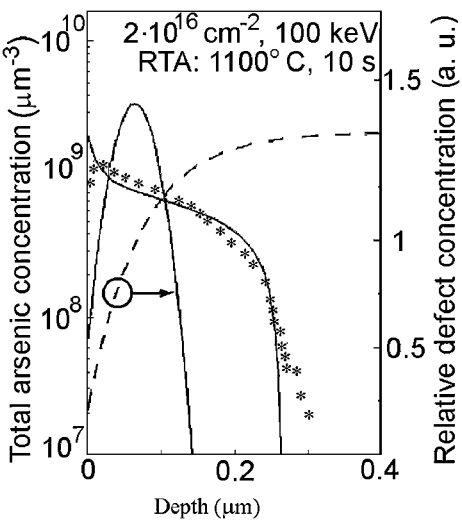

FIG. 2. Calculated arsenic depth profile before and after annealing (continuous lines). Stars mark the experimental data [20]. Dashed line marks the point defect distribution.

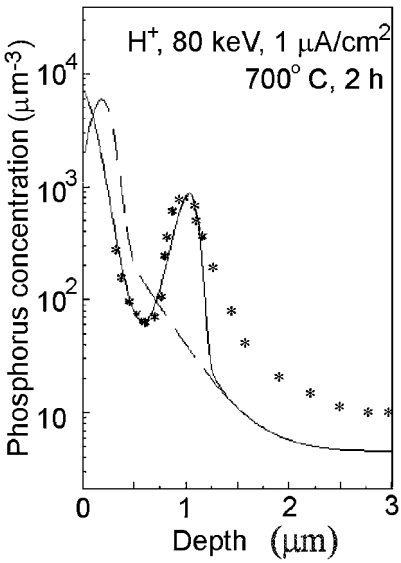

FIG. 3. Calculated phosphorus depth profile after high temperature implantation of hydrogen ions (continuous line). Stars mark the experimental data [22]. Dashed line marks the initial impurity distribution.

was 100 keV, the dose was equal to 2×10^{16} ion/cm^2. The annealing was carried out at a temperature of 1100°C during 10 s. The following values of the parameters that describe the diffusion of impurity atoms and intrinsic point defects were used in modeling: $D_i = 3.36 \times 10^{-6}$ μm^2/sec, $\beta_1 = 1.049$, $\beta_2 = 0.105$, $\tilde{C}_g = 1.5$. The surface defect concentration $\tilde{C}_s = 0.2$. Model and data [21] were used for the description of clustering phenomena: $C^T = C + \beta^{AC} C^4$, $\beta^{AC}(T) = 7 \times 10^{-33} \exp(1.05/k_B T)$ μm^{-3}.

It can be seen in Fig. 2 that the calculated arsenic profile agrees well with experimental data. Note that the effect of point defect absorption on the surface of the semiconductor allows one to explain the region of the impurity uphill diffusion in the vicinity of the interface.

The results of simulation of phosphorus enhanced diffusion during high temperature implantation of hydrogen ions are shown in Fig. 3. For comparison, the experimental data obtained in [22] are used. These experimental results satisfy the requirements of a low level of silicon doping and are characterized by a significant uphill diffusion. Silicon substrates of ⟨111⟩ orientation, n-type, with conductivity of 100 Ωcm were implanted by phosphorus ions with an energy of 140 keV and a dose of 1.4×10^{12} ion/cm^2. Thermal processing in argon ambient at 750°C during 30 minutes was applied for the activation of the dopant and radiation defect annealing. The substrates, implanted by phosphorus, were afterward bombarded by hydrogen ions with the energy of 80 keV and proton current density of 1 μA/cm^2 at the temperature of 700°C. The phosphorus profiles were measured by the differential C-V technique.

To simulate the radiation enhanced diffusion of phosphorus, the initial distribution of ion-implanted impurity was calculated as Pearson IV distribution [13]. In order to describe the extended "tail" of the initial impurity profile, we considered the migration of nonequilibrium phosphorus interstitials. To provide an adequate modeling of radiation enhanced diffusion of phosphorus, it is necessary to establish the type of defects which are responsible for impurity transport and to calculate the spatial distribution of these defects. It is well known that phosphorus diffusion at high surface concentration shows several features that

are characteristic of the surface depth. For example, the enhanced diffusion of impurity atoms occurs in the low-doped region and in the bulk of the semi-conductor. It has been experimentally verified that this enhanced diffusion is a result of the supersaturation of the bulk of the semiconductor by self-interstitials [7]. Supersaturation also increases the intensity of impurity transport by the mechanism of formation, migration, and dissociation of phosphorus-interstitial pairs [11]. It is logical to assume that phosphorus radiation enhanced redistribution under conditions of hydrogen ion implantation is also caused by generation of nonequilibrium silicon self-interstitials. At the same time, we cannot exclude the possibility of vacancy participation in the phosphorus transport since the vacancies are also generated by light ion implantation.

We assume that the process of point defect generation is determined by the energy loss of protons. We calculate the profile of the generation of such defects using tables [13]. The defect generation parameters obtained in [13] have the following values: $R_p^d = 0.75\ \mu$m, $\Delta R_p^d = 0.6113\ \mu$m, $S_k = -1.3$, $R_m^d = 0.9551\ \mu$m. It follows from the value of R_m^d that the maximum of defect generation coincides with the position of the minimum on the phosphorus profile represented in Fig. 3. As follows from Eq. (1), in the case of nonuniform defect distribution the region of the maximum defect concentration is depleted by dopant as a result of the diffusion of impurity atoms. It means that we have determined the parameters of the defect generation rate distribution correctly. Using the obtained values we can solve the point defect diffusion equation. The calculated profiles of self-interstitials concentration and phosphorus concentration before and after hydrogen high temperature implantation are shown in Fig. 3. The calculated results agree well with experimental data, including the region of significant uphill diffusion. The discrepancy of the calculated profile with experimental results takes place only in the region where the impurity concentration decreases. Possible explanations of this observed discrepancy include unaccounted additional diffusion flux of impurities arising due to annealing of radiation defects generated by previous phosphorus implantation and inaccuracy of the C-V characteristics method.

The good agreement of the one-dimensional calculations with experimental results allows us to use these algorithms in predicting impurity distributions in the active regions of designed semiconductor devices. Figure 4 shows the calculated two-dimensional distribution

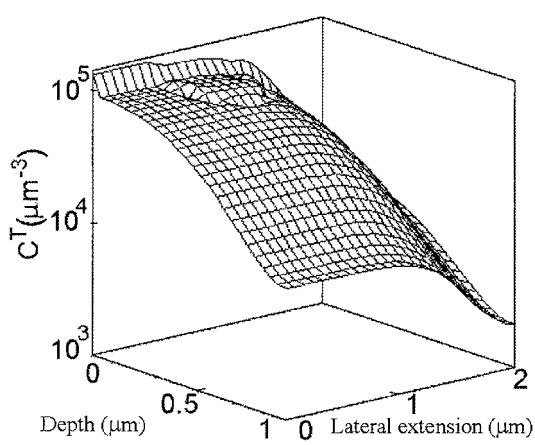

FIG. 4. Boron distribution after a drive-in during 9 h at 1200°C and rapid thermal annealing during 10 s at 1100°C. The implantation energy of boron is 80 keV, the dose is 5×10^{12} ion/cm^{-2}.

of boron in the "well" region of MISFET. We assume that boron implantation was used for the formation of the "well" region and that arsenic implantation was applied for the doping of the "source" and "drain" regions. The silicon substrate was annealed to repair the damage and activate the dopant atoms after implantation. We consider the processes of ion implantation and annealing in more detail. Silicon substrates SEP-20 doped by phosphorus with a concentration of 25 μm^{-3} were used. Boron ions of 80 keV energy were implanted at room temperature to the dose of 0.5×10^{13} ion/cm^2. The width of the mask window was equal to $2a = 3$ μm. It follows from established tables [13] that the parameters of the boron spatial distribution are $R_p = 0.247$ μm, $\Delta R_p = 0.0648$ μm, $S_k = -1$, $\Delta y = 0.076$ μm. The annealing temperature was $T = 1200$°C; the duration was 9 hours. The following values of the parameters that describe ion-implanted boron diffusion were used: $D_i = 1.525 \times 10^{-6}$ μm^2/s, $\beta_1 = 1.355$ [23]. The expression $C^{AC}/C^* = 12(C^{AC}/C^*)^{12}$ was used to describe boron clustering [23]. For this temperature, the calculated value of characteristic impurity concentration C^* was equal 4.08×10^8 μm^{-3}. In view of the rather small dose of ion implantation, high temperature, and long duration of annealing, it was supposed that the point defect distribution during heat treatment was nearly uniform and $\tilde{C}(\mathbf{x}) = \mathbf{1}$. Reflecting boundary conditions were chosen for solving the impurity diffusion equation. After boron annealing, the implantation of arsenic ions with an energy of 100 keV and a dose of 2×10^{16} ion/cm^2 was carried out for the doping of the source and drain regions. The width of the mask window was equal to $2a = 0.5$ μm. The parameters of the ion spatial distribution were $R_p = 0.0644$ μm, $\Delta R_p = 0.023$ μm, $S_k = 0.4$, $\Delta y = 0.0173$ μm [13]. After implantation the rapid annealing was carried out at a temperature of 1100°C during 10 s. In simulation of annealing the following values of the parameters that describe the impurity atom diffusion were used: $D_i = 3.36 \times 10^{-6}$ μm^2/s, $\beta_1 = 1.049$ and $\beta_2 = 0.105$ for arsenic [20]; $D_i = 1.517 \times 10^{-5}$ μm^2/s and $\beta_1 = 1.8189$ [23] for boron.

The values obtained in the one-dimensional model of ion-implanted arsenic redistribution were used in the simulation to account for the nonuniformity of the point defect distribution and the deviation of the defect concentration from thermal equilibrium in the case of rapid thermal annealing. Similar to the one-dimensional case, we suppose that the relative defect concentration on the surface $\tilde{C}_s = 0.2$, the average defect diffusion length $l_i = 0.07$ μm, and the value of the relative defect generation rate $\tilde{C}_g = 1.5$. Reflecting boundary conditions have been chosen for solving the impurity diffusion equation.

It is seen in Fig. 4 that the regions of significant uphill diffusion are observed in the vicinity of the semiconductor surface and in the domain doped with arsenic. The maximum formation of impurity concentrations in the vicinity of the surface are caused by absorption of defects on the interface. The formation of the high concentration boron region at the place of arsenic location is caused by the drift of point defects and "impurity-defect" pairs in the internal electrical field existing in the region of strong nonuniform distribution of the donor impurity.

The calculated two-dimensional distribution of arsenic after rapid thermal annealing together with the previously obtained boron distribution are plotted in Fig. 5. The figure shows that the nonuniform distribution of point defects in the case of reflecting boundary condition also leads to the formation of an arsenic concentration maximum in the vicinity of the interface. It is important to note that in the two-dimensional case significant arsenic lateral diffusion occurs.

Finally, we investigate the case of local redistribution of impurity atoms in the previously formed semiconductor structure shown in Fig. 4. We use local high temperature

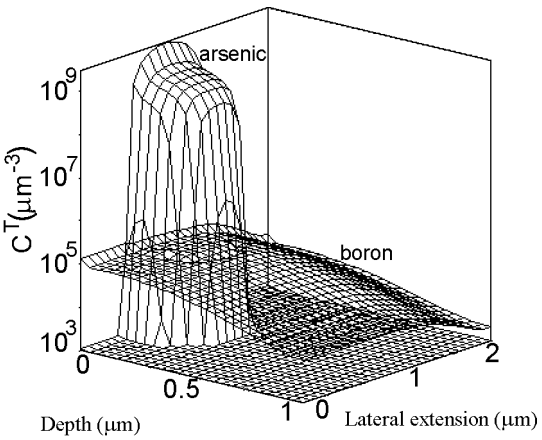

FIG. 5. Arsenic distribution after rapid thermal annealing during 10 s at 1100°C. The implantation energy is 100 keV; the dose is 2×10^{16} ion/cm^{-2}.

implantation of hydrogen ions for this purpose. The results of two-dimensional simulations of local transformation of impurity atom distributions during such treatment are shown in Figs. 6 and 7 for the width of the hydrogen implantation windows $2a = 0.4$ μm and $2a = 2.3$ μm, respectively. The hydrogen ions were implanted with the energy of 10 keV within one hour. The substrate temperature was supported equal to 625°C, which is enough for radiation enhanced diffusion. As follows from the tables [13], the parameters of spatial distribution of hydrogen atoms in silicon are $R_p = 0.1366$ μm, $\Delta R_p = 0.0555$ μm, $S_k = -1.45$, $\Delta y = 0.0572$ μm. It was supposed that the hydrogen implantation was carried out through a thin layer deposited on the surface of the semiconductor. In this case, the maximum of defect generation is located at the distance Δx below the interface. The following parameters describing the diffusion redistribution of impurity are used in the computation: $D_i = 3.168 \times 10^{-13}$ μm^2/s, $\beta_1 = 0.067$, and $\beta_2 = 5.67 \times 10^{-4}$ [20] for arsenic; $D_i = 2.913 \times 10^{-12}$ μm^2/s, $\beta_1 = 17.92$ for boron [23].

Proceeding from the results of the previous calculations, the following values of the parameters that describe the defect subsystem state were chosen: the average defect migration

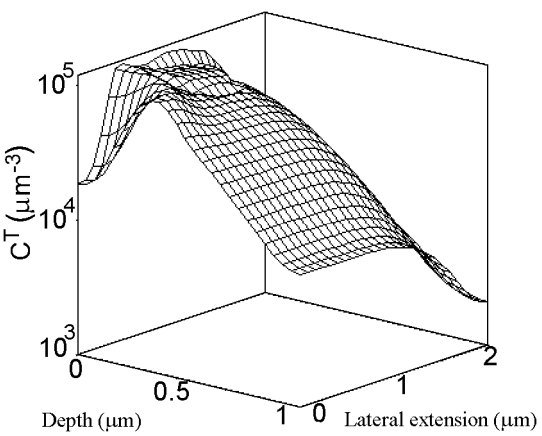

FIG. 6. Boron distribution after high temperature ion implantation during 1 h at 625°C. The hydrogen ion energy is 10 keV; the window width is $2a = 0.4$ μm.

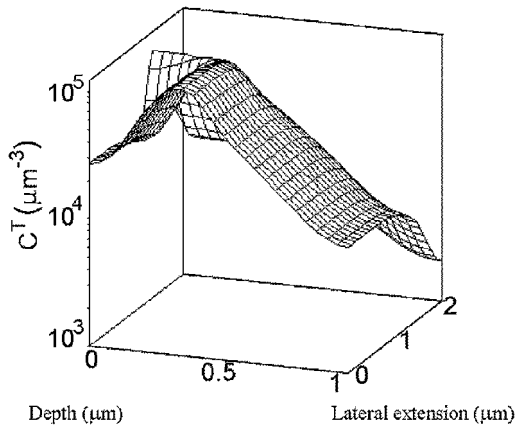

FIG. 7. Boron distribution after high temperature ion implantation during 1 h at 625°C. The hydrogen ion energy is 10 keV; the window width is $2a = 2.3$ μm.

length $l_i = 0.1$ μm, the value of the relative defect generation rate $\tilde{C}_g = 10^7$. For the given point defect generation rate the value of the average impurity diffusion length

$$L = \sqrt{D_i t \tilde{C}_{\max}} = 0.1\,\mu\text{m}$$

is used, which is close to the value $L = 0.85$ μm obtained in the case of simulation of phosphorus radiation enhanced diffusion shown in Fig. 4.

Reflecting boundary conditions at the interface are used for both impurity atoms and point defects. The typical results of calculations of the spatial distribution of point defects for this boundary condition of the mask window width $2a = 2.3$ μm are shown in Fig. 8. The calculated distribution of point defects corresponds to the process of impurity redistribution represented in Fig. 7.

As it can be seen from Figs. 6 and 7, the high temperature implantation of hydrogen ions allows one to modify the distribution of boron atoms in the channel region of MISFET widely used in microelectronics. For example, the radiation enhanced diffusion allows one to considerably lower the boron concentration in the channel region near the surface of the

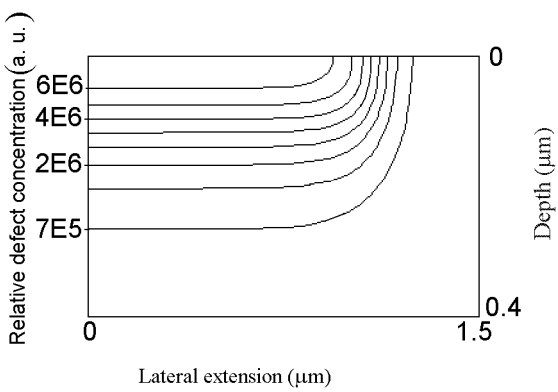

FIG. 8. Defect distribution for high temperature implantation of hydrogen atoms. The window width is $2a = 2.3$ μm.

semiconductor. Simultaneously, there is a significant increase in the boron concentration in a narrow layer beyond the defect generation region, where the enhanced diffusion of impurity atoms occurs. Thus, the super-steep retrograde-channel profile is formed. This helps to create a highly conducting layer when the transistor is turned "on." The latter phenomenon is very important for advanced device fabrication [1]. Besides, double implantation of boron can be excluded in MISFETs manufacturing. It is important to note that the calculations presented show an opportunity for the formation of other specific spatial distributions of impurity. In all cases, the redistribution of impurity atoms takes place in the strictly assigned local domain, whose dimensions can be easily controlled by varying the implantation energy and mask window geometry.

5. CONCLUSION

A model of electrically active impurity diffusion in semiconductor crystals has been formulated on the basis of nonequilibrium thermodynamics. The nonuniformity of point defect distributions in ion-implanted layers and in the vicinity of semiconductor interfaces is taken into consideration in the model. A set of generalized transport equations that describe coupled diffusion of impurity atoms and point defects in semiconductor crystals is obtained. Several impurities of different conductivity type are considered. The method of solving these nonlinear two-dimensional equations enables rapid and sufficiently accurate numerical solution. The corresponding simulation code DIPRAM enables the computation of various doping processes, including radiation enhanced diffusion of dopants during high temperature ion implantation and transient enhanced diffusion of impurity atoms during rapid thermal annealing of ion-implanted layers. For each considered example, the time of computing does not exceed 4 min on a PC Pentium II/350 for a 100×200 space grid. The calculations show that specific space transformations of already formed doped regions of semiconductor devices can take place as a result of radiation enhanced diffusion during high temperature implantation of hydrogen ions. A controlled local transformation of impurity distributions can be achieved, since the redistribution of impurity takes place only in the region of generation and diffusion of point defects, but not in other zones. This local transformation phenomenon can be used in various branches of IC manufacturing. For example, the directed modification of the impurity distribution in the channel region of a MISFET can be carried out.

ACKNOWLEDGMENT

The work reported here was supported in part by the COBASE (Collaboration in Basic Science and Engineering).

REFERENCES

1. P. A. Packan, Scaling transistors into the deep-submicron regime, *MRS Bulletin/June 2000* **25**, 18 (2000).
2. N. Cowern and C. Rafferty, Enhanced diffusion in silicon processing, *MRS Bulletin/June 2000* **25**, 39 (2000).
3. H. Ryssel, and I. Ruge, *Ionenimplantation* (Wiley, New York, 1986).
4. X. Deng and B. L. Sopori, Low-temperature diffusivity of hydrogen in silicon substrates, *Mat. Res. Soc. Symp. Proc.* **378**, 359 (1995).
5. G. V. Gadiyak, Physical model and numerical results of dissociation kinetics of hydrogen-passivated Si/SiO_2 interface defects, *Thin Solid Films* **350**, 147 (1999).

6. M. Jaraiz, G. H. Gilmer, J. M. Poate, and T. D. de la Rubia, Atomistic calculation of ion implantation in Si: Point defects and transient enhanced diffusion phenomena, *Appl. Phys. Lett.* **63**, 409 (1996).
7. M. Uematsu, Simulation of boron, phosporus, and arsenic diffusion in silicon based on an integrated diffusion model, and the anomalous phosphorus diffusion mechanism, *J. Appl. Phys.* **82**, 2228 (1997).
8. M. E. Law, G. H. Gilmer, and M. Jaraiz, Simulation of defects and diffusion phenomena in silicon, *MRS Bulletin/June 2000* **25**, 45 (2000).
9. P. Baruch, J. Monnier, B. Blanchard, and C. Castaing, Redistribution of boron in silicon through high-temperature proton irradiation, *Inst. Phys. Conf. Ser. No.* **23**, 453 (1975).
10. Ch. Lucas, J. P. Gailliard, S. Loualiche, P. Baruch, J. C. Pfister, and R. Truche, in *Defects and Radiation Effects in Semiconductors,* edited by J. H. Albany (The Institute of Physics, London, 1979), p. 551.
11. O. I. Velichko, A set of coupled equations for modeling of radiation-enhanced diffusion of ion-implanted impurities, *Radiotechnika i Elektronika (Belarus)* **14**, 91 (1985).
12. V. A. Labunov, and O. I. Velichko, Generalized diffusion equation for impurity atoms in semiconductor crystals, *J. Eng. Phys.* **57**, 1351 (1989).
13. A. F. Burenkov, F. F. Komarov, M. A. Kumahov, and M. M. Temkin, *Space Distribution of Energy Deposited in Atomic Collisions in Solids* (in Russian) (Energoatomizdat, Moscow, 1985).
14. V. A. Labunov, O. I. Velichko, and S. K. Fedoruk, Simulation of diffusion of magnesium in gallium arsenide. I. Thermal diffusion of Mg in $Al_XGa_{1-X}As$, *J. Eng. Phys. Thermophys.* **67**, 1067 (1994).
15. D. A. Anderson and M. M. Rai, The use of solution adaptive grids in solving partial differential equations, *Appl. Math. Comput.* **10**, 317 (1982).
16. N. N. Yanenko, *The Method of Fractional Steps* (Springer-Verlag, New York, 1971).
17. R. L. Minear, D. C. Nelson, and J. F. Gibbons, Enhanced diffusion in Si and Ge by light ion implantation, *J. Appl. Phys.* **43**, 3468 (1972).
18. R. Richtmyer and K. Morton, *Difference Methods for Initial-value Problems* (Wiley, New York, 1967).
19. W. Hackbusch, *Multi-grid Methods and Applications,* Springer Series in Computational Mathematics (Springer-Verlag, Berlin, 1985), Vol. 4.
20. R. Kögler, E. Wieser, G. Otto, and P. Knothe, Rapid thermal annealing of high dose arsenic-implanted silicon, *Appl. Phys. A.* **51**, 53 (1990).
21. K. Tsukamoto, Yo. Akasaka, and K. Kiima, Thermal diffusion of ion-implanted arsenic in silicon, *Jap. J. Appl. Phys.* **19**, 87 (1980).
22. W. Akutagawa, H. L. Dunlap, R. Hart, and O. J. Marsh, Impurity-peak formation during proton-enhanced diffusion of phosphorus and boron in silicon, *J. Appl. Phys.* **50**, 777 (1979).
23. A. N. Bubennikov, *Simulation of Integrated Microtechnology, Devices, and Circuits* (in Russian) (Vysshaia Shkola, Moscow, 1989).